Water Research 254 (2024) 121306

Contents lists available at ScienceDirect

Water Research

journal homepage: www.elsevier.com/locate/watres

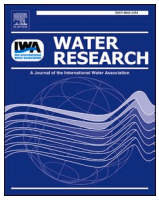

On the vertical structure of non-buoyant plastics in turbulent transport

James Lofty [a,**], Daniel Valero [b,c,d,*], Antonio Moreno-Rodenas [e], Biruk S. Belay [f], Catherine Wilson [a], Pablo Ouro [g], Mário J. Franca [b]

[a] Cardiff University, School of Engineering, Hydro-Environmental Research Centre, Wales, UK
[b] Karlsruhe Institute of Technology, Institute of Water and Environment, Karlsruhe, Germany
[c] Water Resources and Ecosystems Department, IHE Delft, Delft, the Netherlands
[d] Presently: Imperial College London, Civil and Environmental Department, London, UK
[e] Deltares, Hydraulic Engineering Department, Delft, the Netherlands
[f] Hydraulic Engineering Chair, Helmut Schmidt University, Hamburg, Germany
[g] School of Mechanical, Aerospace and Civil Engineering, University of Manchester, Manchester, UK

ARTICLE INFO

Keywords:
Macroplastic
Rouse number
Settling velocity
Bed load
Pollution
Plastic

ABSTRACT

Plastic pollution is overflowing in rivers. A limited understanding of the physics of plastic transport in rivers hinders monitoring, the prediction of plastic fate and restricts the implementation of effective mitigation strategies. This study investigates two unexplored aspects of plastic transport dynamics across the near-surface, suspended and bed load layers: (i) the complex settling behaviour of plastics and (ii) their influence on plastic transport in river-like flows. Through hundreds of settling tests and thousands of 3D reconstructed plastic transport experiments, our findings show that plastics exhibit unique settling patterns and orientations, due to their geometric anisotropy, revealing a multimodal distribution of settling velocities. In the transport experiments, particle-bed interactions enhanced mixing beyond what established turbulent transport theories (Rouse profile) could predict in low-turbulence conditions, which extends the bed load layer beyond the classic definition of the bed load layer thickness for natural sediments. We propose a new vertical structure of turbulent transport equation that considers the stochastic nature of heterogeneous negatively buoyant plastics and their singularities.

1. Introduction

The production of plastics is expected to double by 2040, (Geyer et al., 2017) leading to mounting challenges due to the accompanying increase in plastic leakage into the environment (Bergmann et al. 2022). This escalation is particularly concerning in light of growing scientific evidence showing that plastic pollution is causing unprecedented impacts to many aspects of life, including biodiversity, food security and climate change (De-la-Torre 2020; MacLeod et al., 2021; Clark et al. 2023). Moreover, plastics have the potential to pose risks to human health (Dick Vethaak and Legler 2021), an unsettling revelation further emphasised by recent studies detecting plastics in human lung tissue (Jenner et al., 2022), the placenta (Amereh et al. 2022; Ragusa et al. 2022) and blood (Leslie et al., 2022).

In response to these concerns, the United Nations Environment Programme has signed a legally binding treaty involving 175 member states aimed at promoting measures to globally reduce plastic pollution in the environment, beginning as early as 2024 (UNEP 2023). Central to these efforts are the proposed expansion of monitoring programs for plastic pollution in rivers to inform and influence policy (UNEP 2021). However, current monitoring protocols lack harmonisation and inter-comparability across basins (González-Fernández and Hanke 2017; Hurley et al. 2023). Moreover, the complexity and variability inherent to fluvial plastic transport dynamics are not yet well understood (Waldschläger et al. 2022; Lofty et al., 2023a). This lack of comprehensive knowledge significantly impedes our ability to quantify riverine plastic budgets and frequently leads to significant underestimations of plastic concentrations. For example, current riverine monitoring strategies may fail to detect as many as 90 % of plastics residing in the river water column for flows with strong turbulence, according to estimations presented by Valero et al. (2022).

An additional challenge to existing fluvial plastic monitoring

* Corresponding author at: Imperial College London, Civil and Environmental Department, London, UK
** Corresponding author at: Cardiff University, School of Engineering, Hydro-Environmental Research Centre, Wales, UK
E-mail addresses: Loftyj@cardiff.ac.uk (J. Lofty), d.valero@imperial.ac.uk (D. Valero).

https://doi.org/10.1016/j.watres.2024.121306
Received 20 November 2023; Received in revised form 24 January 2024; Accepted 10 February 2024
Available online 13 February 2024

strategies is that current methods primarily focus on water surface observations (González-Fernández and Hanke 2017; Geraeds et al., 2019; van Emmerik and Schwarz 2020; Kataoka and Nihei 2020; Vriend et al., 2020). As a result, a large portion of negatively buoyant plastics may remain undetected during monitoring efforts, leading to a consistent bias in river pollution estimates. This becomes especially troublesome given that studies have shown that the prevalence of plastics transported in the near-bed region of rivers might be comparable to that of floating plastics (Blondel and Buschman 2022; McGoran et al., 2023; Vriend et al., 2023) and this transport layer may have even more complex dynamics due to bedform interactions (Russell et al., 2023).

Describing the behaviour and quantifying the concentration of suspended particles in turbulent river-like flows, such as sediments and plastic particles (originally as laboratory proxy for natural sediments), has been studied since the work of Rouse (1939). Rouse derived a concentration profile of suspended point-particles as a function of the relative settling velocity of a particle and turbulence forces, which can be expressed by the Rouse number β (Rouse 1939):

$$\beta = \frac{w}{\kappa u_*} \tag{1}$$

where w is the settling velocity of the particle, $\kappa = 0.41$ is the von Kármán constant and u_* is the shear velocity. The Rouse number β determines the shape of the Rouse profile, which is a theoretical vertical concentration profile for point-particles in turbulent flows, under the assumption of parabolic and symmetric eddy diffusivity distribution across the water column. The Rouse profile (Rouse 1939) can be expressed as:

$$\frac{C}{C_a} = \left[\left(\frac{H-z}{z}\right)\left(\frac{a}{H-a}\right)\right]^{\beta} \tag{2}$$

where C is the concentration at a height z above the bed, C_a is a reference concentration at $z = a$ and H is the flow depth. This model has been described in detail for vertical concentration profiles of neutrally (Elata and Ippen 1961) and negatively (Rashidi et al., 1990; Kaftori et al., 1995; Muste et al., 2005; Baker and Coletti 2021) buoyant point-particles, which have material compositions including quartz sediment and plastic.

Recently, turbulent transport theories have been suggested for application within plastic pollution transport (Cowger et al., 2021; Lofty et al., 2023b; Yu et al., 2023). Turbulent suspension has been described for positively buoyant macroplastic (plastics $>$ 5 mm in size) of different shapes (Valero et al., 2022) and near-spherical microplastics (plastics $<$ 5 mm in size) (Born et al., 2023). Given the diversity of plastic pollution, in terms of shape and geometry anisotropy, it may be expected that vertical concentration profiles of plastics may depart from that calculated by the Rouse profile, due to simplicities in the derivation of the Rouse equation (Eq. (1)), which do not consider different fluid drag components related to different particle orientations (Baker and Coletti 2022) or particle inertia near the bed (Baker and Coletti 2021). However, in the study by Valero et al. (2022), the observed plastic vertical concentration profiles did not statistically deviate from a Rouse profile within experimental uncertainty, until immediately beneath the free surface, where a new surfaced transport layer of plastic was observed. In this near-surface layer, transport is described by the balance of relative settling/rising velocity of a particle, turbulence and surface tension, and thus observed plastic concentrations exceed the theoretical Rouse profile estimates, as only the former two factors are considered.

The settling velocity is thus an essential descriptor for plastic transport (Eq. (1)) (Waldschläger and Schüttrumpf 2019; Kuizenga et al., 2022; Goral et al. 2023), which has been studied for plastic particles, at least, since the study by Christiansen and Barker (1965). If the settling velocity of a sampled plastic is known, as well as the river hydrodynamics, the Rouse number can be used in predictive models to explain plastic concentration in the river water column from a single sampling point at a given depth (Cowger et al., 2021). Therefore, a suitable settling velocity parameter needs to be carefully measured in order to calculate appropriate vertical concentration profiles of the plastic particle.

Typically, when conducting settling experiments, one settling velocity is taken deterministically as a singular ensembled average value based on a number of settling tests repeats. However, given the diversity of plastics, with varying geometric anisotropy and shape, plastics may find distinct orientations during their vertical transport, which can affect their equilibrium settling state and subsequent settling velocity. Here we hypothesize that these different settling orientations may have different levels of stability, i.e., one mode being more stable than the others, which are therefore metastable. When a plastic particle is in a metastable position, and is subject to a large enough perturbation, the plastic may abruptly move into a new metastable or stable position, resulting in a different exposed area and drag force, which affects the plastic's vertical transport. Each orientation can therefore correspond to a distinct fall velocity, resulting in a multimodal settling distribution. Similar results have been observed for cards (Andersen et al., 2005), disks (Field et al., 1997; Auguste et al., 2013) and cylinders (Jayaweera and Mason 1965), where multiple metastable and stable settling orientations during their vertical transport have related to distinct equilibrium settling velocities. However, this aspect of vertical transport dynamics has yet to be addressed from a plastic transport perspective. In light of this, a pertinent question arises: how will the different modes of settling impact plastic transport in river-like turbulent flows?

Two unresolved aspects of plastic transport are therefore investigated in this study: i) the role of multimodality in shaping the distribution of settling velocities for negatively buoyant macroplastics with varying geometric anisotropy, and ii) the resulting impact on their vertical concentration and transport within river-like flows. To unravel these intricate mechanisms, an extensive investigation involving hundreds of negatively buoyant samples was conducted. The samples are based on full and deformed polystyrene drinking cups, as well as cups that have been cut half-wise and into fragments. The samples thus encompassed four distinct types of plastic, each varying in size, shape, and anisotropy and are representative of commonly observed plastics in the river environment (van Emmerik et al. 2018; van Emmerik et al. 2020a; Nguyen and Bui 2023). A total of 400 settling experiments were conducted to first assess the multimodality in settling plastic. We then assembled three-dimensional transport trajectories from video recordings of approximately 3000 plastic samples transported under turbulent river-like flows. By comparing their vertical concentration profiles to the theorical Rouse profile (Eq. (2)), distinct features of the multimodal distribution of plastic settling that better explain observed concentration profiles were identified.

2. Methods

2.1. Experimental design

Experiments were conducted in two laboratories. Measurements of the settling velocity of plastics samples were conducted in the Theodor Rehbock hydraulics laboratory at Karlsruhe Institute of Technology (Germany) and the plastic transport experiments, conducted under turbulent flow conditions, were undertaken in the Hydraulic Engineering Laboratory at Delft University of Technology (the Netherlands). For the plastic settling experiments, it was apparent that the plastic samples settled at different velocities, which was related to different trajectories and settling orientations. Therefore, experiments in which plastic samples settled in straight vertical trajectories and had little interactions with the tank walls were conducted in a cylindrical settling tank, 188 cm in height and 24 cm in diameter (tank 1, Fig. 1A), while experiments in which plastic samples settled with an oscillating trajectory and or moved significantly away from the initial drop position were conducted in a wider rectangular tank, 98 cm in height (z), 200 cm in length (x), and 57

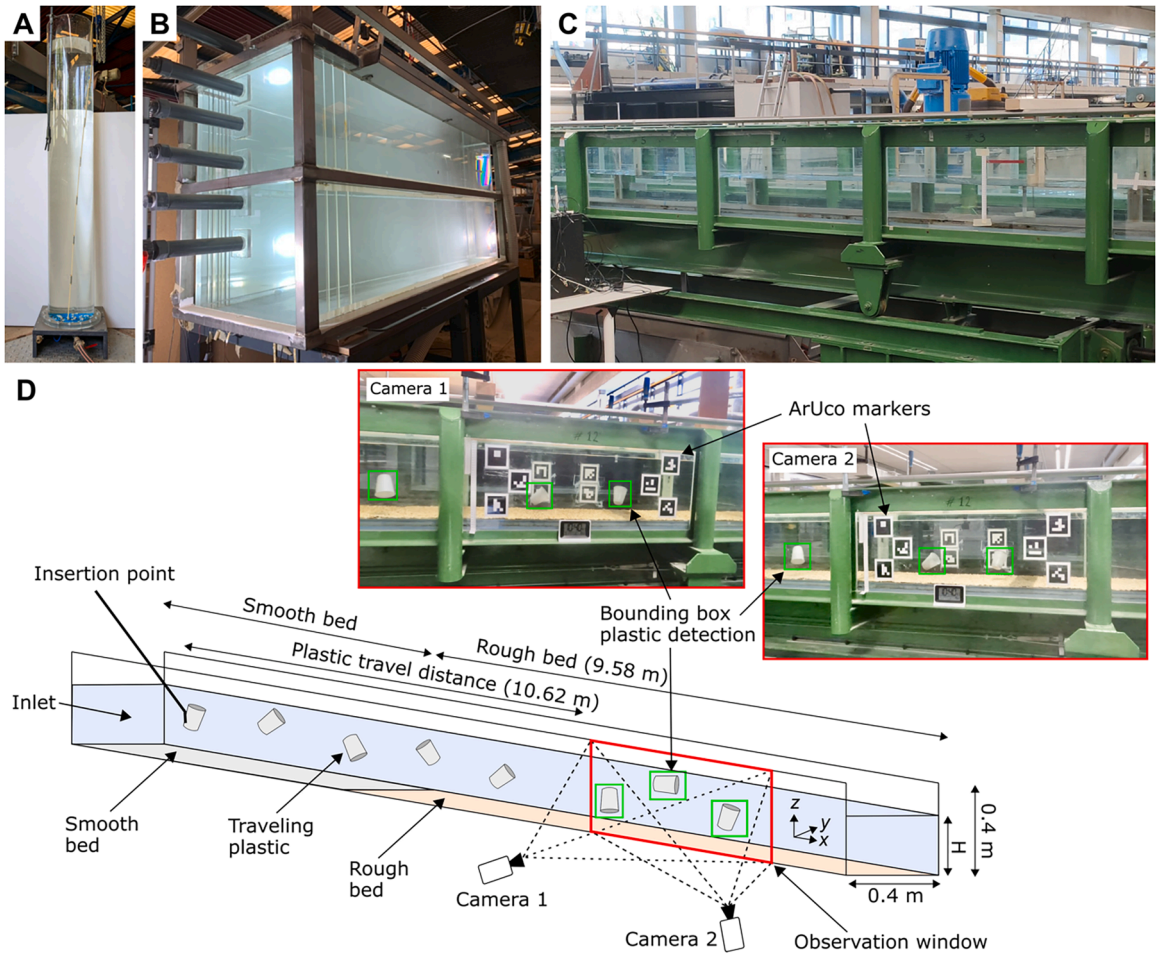

Fig. 1. Photographs of the settling tanks used to measure setting velocities of A) the full and deformed cups, B) the half cups and cup fragments. The wider tank allowed for the settling of samples with higher anisotropy, in which horizontal motion had larger amplitude. C) The open channel flume used for plastic transport experiments. D) Plastic transport experimental setup and bounding box plastic detection output using a synchronous multi-camera detection routine.

cm in width (y) (tank 2, Fig. 1B). Experiments in which particle-wall interactions occurred, and hence affected the settling velocity, were discarded and repeated. Tank 1 was filled up with tap water to a depth of 140 cm, while tank 2 was filled up to a depth of 70 cm. Both tanks were kept at room temperature.

Transport experiments for negatively buoyant plastics were

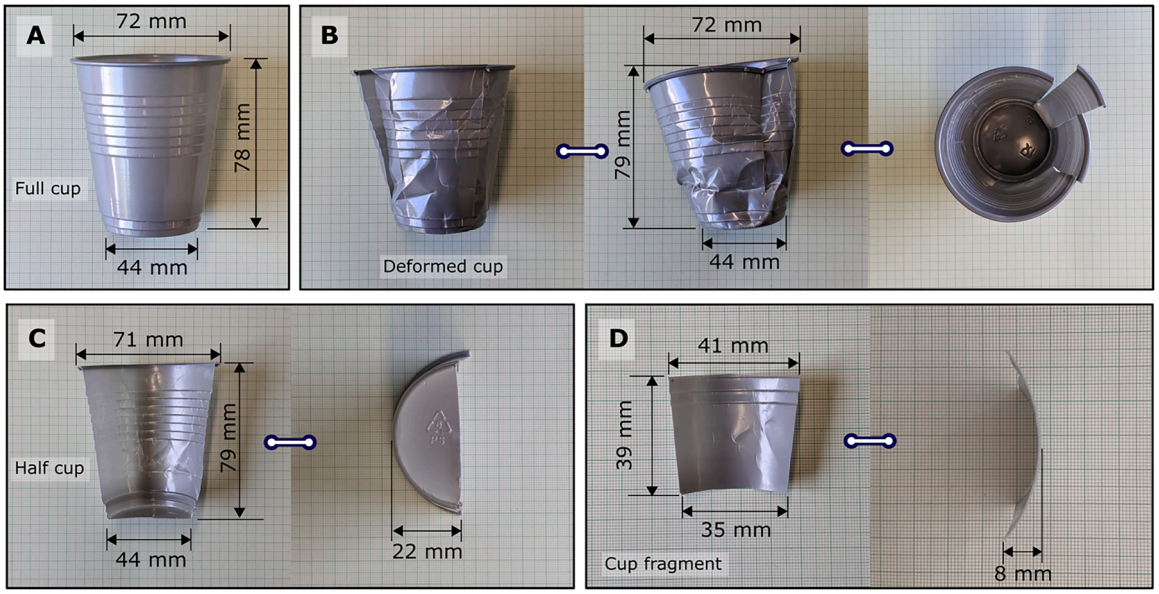

Fig. 2. Photographs of A) full, B) deformed, C) half and D) cup fragments used in experiments with measured dimensions.

conducted in a rectangular open channel flume (Fig. 1C) with the dimensions 14.40 m long, 0.4 m deep, 0.4 m wide, and a bed slope of 0.00026, analogous to the experimental setup of Valero et al. (2022) . A 9.58 m long roughened bed consisting of closely packed sand grains of median diameter of 6.7 mm (see Fig. 2C of Valero et al. (2022) for granulometry curve of sand grains) was installed on the flume floor to increase turbulence in the flow.

Five different flow conditions were considered for the plastic transport experiments and are described in Table 1. All discharges represent subcritical flows with high Reynolds numbers (*Re*) between 353,768 - 1,002,458. Flow depth was controlled by a downstream gate and the flow depth for all flow conditions was measured using a point gauge for each experiment, obtaining a mean value of 0.278 m (± 1 mm, gauge resolution). Flow characterisation was conducted by velocity measurements at 2 cm vertical intervals using an Acoustic Doppler Velocimeter (ADV, Vectrino+, Version 1.24.00) and upstream hydrogen bubble seeding (Blanckaert and Lemmin 2010). Each point was sampled for at least 2 min with a sampling frequency between 100 and 200 Hz, depending on signal quality.

Full open channel flow hydrodynamics, as well as average and turbulent quantities, were described for all flow conditions in Valero et al. (2022) (see Fig. 4 of Valero et al. (2022) for full flow hydrodynamics, which follow expected trends for smooth open channel flow). The shear velocity u_* and the boundary layer thickness were obtained through a log-law fitting and verified by using the Reynolds shear stress profile, as described in Valero et al. (2022). Both methods were in good agreement, but for simplicity, the shear velocity u_* values used for subsequent calculations are only those estimated through a log-law fitting (presented in Table 1).

2.2. Plastic samples

For both settling and transport experiments we consider clean negatively buoyant macroplastic samples (plastics > 5 mm in size, as defined by Hartmann et al. (2019)) which are shown in Fig. 2 and characterised in Table 2. The Corey Shape Factor (CSF) (Corey et al., 1949) is also described in Table 2 to explain the anisotropy of the plastic samples (CSF = 1: isotropic, < 1: anisotropic). The selected plastics were chosen to be representative of riverine plastic litter observations and all originate from the same plastic samples but were fragmented and deformed into different shaped forms. These include undeformed rigid 3D objects (full cups, Fig. 2A), damaged rigid 3D objects (deformed cups, Fig. 2B), rigid quasi-2D fragment (half cups, Fig. 2C) and smaller quasi-2D fragments (cup fragment, Fig. 2D). The full cups were left unaltered from the original packaged state. The deformed cups were formed by crushing full cups against the floor using human weight, while the half cups and the cup fragments were formed by carefully cutting the full cups in half height-wise, and into small uniformly sized fragments, respectively. The main dimensions of the plastic samples are presented in Fig. 2.

The plastic samples were composed of one of the top five most produced plastic polymers (Geyer et al., 2017), namely polystyrene (PS) and belong to the 20 most widely found macroplastics (categorised by the River-OSPAR protocol (van Emmerik et al. 2020b)) found on the Rhine-Meuse delta (van Emmerik et al. 2020a) and Saigon River (Nguyen and Bui 2023) riverbanks, as well as representative of monitoring campaigns in Asian river networks (van Emmerik et al. 2018). The selected samples also represent different levels of fragmentation and degradation, from full unaltered cups to damaged and fragmented cups, therefore, potentially considering different levels of plastic age-related degradation in the river environment.

The density of the plastic samples was determined using a 50 ml pycnometer following ISO 1183–1:2019 (E) for pycnometer tests (ISO 2019) at the water quality laboratory of Deltares (Netherlands). During the tests, distilled water was used as the immersion liquid (997.98 kg/m^3 at 21°C, estimated using the same pycnometer). From each plastic, small fragments were cut to allow insertion in the pycnometer, filling the pycnometer approximately halfway. Displaced volumes and dry weights of the inserted samples allowed estimating the density of the material. The density estimation was repeated five times allowing the plastic's density uncertainty to be estimated, resulting in a density of 1020 ± 0.006 kg/m^3.

2.3. Experimental procedure – settling experiments

To capture the different modes of settling for each of the plastic samples and to decrease statistical uncertainty, 100 settling tests were conducted per plastic sample. Full and deformed cup settling experiments were conducted in tank 1 (Fig. 1A), while half and fragmented cups settling tests were conducted in the larger rectangular settling tank 2 (Fig. 1B), therefore allowing for larger horizontal motions that were observed for the more anisotropic plastics. The plastic samples were released in the centre of each tank, immediately below the water level, very carefully to avoid inducing predefined motions. To avoid systematic biases in the settling orientations of the plastic, samples were released at random orientations to ensure that the complete variability of the plastic settling was represented in the results.

A Logitech C920 camera (1080p Full HD, 30 frames per second) was placed on a tripod facing each of the settling tanks and was used to record the settling of the plastic samples. The plastic trajectories were extracted from each of the video recordings manually every vertical 10 cm for samples settling in tank 1, and 1 cm for samples settling in tank 2. Using the differences between the manually extracted coordinates and time stamps, the settling velocities were obtained (an exemplary routine is included in Lofty (2023)). In the calculation of the sample's settling velocities, the refraction correction was also considered in the velocity estimations, referencing each particle to the central axis of each tank. Transformation from pixel coordinates to real distance was performed with a multi-point linear transformation.

Inspection of the plastic trajectories allowed for verification that plastics reach an equilibrium settling state that was independent of the release point; i.e., the settling velocity and orientation no longer change over the immediate trajectory. Thereafter, the settling velocity is determined through the time it takes a given sample to travel a segment of 30 cm vertically (between 90 and 120 cm for tank 1 and 10 to 40 cm for tank 2, relative to the water level). Although the orientation of the settling samples can vary during the trajectories, a mode of settling was determined by visual inspection of distinct orientation of the plastic

Table 1
Flow conditions used in transport experiments including the total discharge (Q), uncertainty in its estimation (ε_Q), specific discharge (q), Froude number ($F = U/\sqrt{gH}$, where U is the depth-averaged velocity), and Reynolds number ($Re = 4q/\nu$, with ν the water kinematic viscosity). Shear velocity u_* and boundary layer thickness δ correspond to the log-wake law profile fit.

Q (m^3/s)	ε_Q (%)	q (m^2/s)	H (m)	U (m/s)	F (-)	Re (-)	u_* (m/s)	δ (m)
0.035	3.21	0.088	0.278	0.318	0.193	353,768	0.0213	0.111
0.053	1.80	0.132	0.278	0.475	0.288	528,405	0.0320	0.116
0.073	2.34	0.183	0.278	0.657	0.398	730,843	0.0444	0.105
0.088	2.49	0.219	0.278	0.787	0.477	875,200	0.0535	0.106
0.100	2.24	0.251	0.278	0.901	0.546	1002,458	0.0613	0.102

Table 2
The material and geometrical properties of the plastic samples used in experiments including the plastic density (ρ_p), maximum (L_1), intermediate (L_2) and smallest (L_3) dimensions of the plastic samples, the Corey Shape Factor (CSF) (Corey et al., 1949), calculated as $\frac{L_3}{\sqrt{L_1 L_2}}$, the maximum diagonal length (λ) calculated as $\lambda = (L_1^2 + L_2^2)^{1/2}$, the plastic volume ($V_p$), estimated from mass and density, and the remaining volume (herein, ΔV_p) compared to the largest volume sample (i.e., full cup).

Plastic	Class	ρ_ρ (± std) (kg/m^3)	L_1 corresponds to	L_1 (mm)	L_2 corresponds to	L_2 (mm)	L_3 corresponds to	L_3 (mm)	CSF	λ (mm)	V_p (mm^3)	ΔV_p (%)
Full cup	Rigid 3D body	1020 ± 6	Height	78	Largest diameter	72	Smallest diameter	44	0.59	106	3429.2	100
Deformed cup	Damaged rigid 3D body	1020 ± 6	Height	79	Largest diameter	72	Smallest diameter	44	0.58	107	3399.3	99.1
Half cup	Rigid quasi-2D fragment	1020 ± 6	Major side	79	Largest diameter	71	Smallest diameter	22	0.29	106	1696.7	49.5
Cup fragment	Smaller rigid quasi-2D fragment	1020 ± 6	Side	41	Side	39	Concavity height	8	0.20	57	277.6	8.09

sample from the recorded videos at a reference vertical position where the samples remain in an equilibrium state. This was deemed to be at 110 cm vertical distance from the release position for full and deformed cups (tank 1) and 25 cm for half cups and cup fragments (tank 2), relative to the water level.

2.4. Experimental procedure – transport experiments

For the plastic transport experiments, samples were released one at a time at an insertion point set at the upstream end of the open channel flume by a controlled distance grabber at around 20 – 30 % of the water depth (Fig. 1D). This upstream insertion point allowed plastics to interact with the wall-generated turbulent flow. A sample number of $N = 150$ for each plastic class (full, deformed, half and fragmented cups) was targeted for each of the five flow conditions, although a small number of samples were lost during transport (stuck in the channel glass or rough bed surface) or remained undetected. Plastics were cleared from bubbles before being released into the flume using the same procedure as Valero et al. (2022). This prevented most of the bubbles from remaining attached to the plastic sample. The contribution of any remaining bubble to buoyancy is deemed negligible (Appendix B of Valero et al. (2022)).

The plastic samples travel a longitudinal downstream distance of 10.62 m before reaching the observation window, where four GoPro HERO9 cameras (Sony IMX677 CMOS sensor, 60 frames per second) recorded the movement and position of the plastic travelling through the observation window (Fig. 1D) (see supplementary videos for example analysis). Two of the cameras were positioned in a vertical plane in front of the observation window, at two different angles, and were also aligned with the water surface to accurately capture any plastics interacting with the free surface during the tests. This positioning also avoided reflections in the lower free surface, which would hamper the automated tracking of plastics. The cameras were initiated by a common IR remote trigger and an external flashlight was used to perform accurate cross-camera time-synchronisation. The camera distortion and calibration methodology are analogous to techniques used in Valero et al. (2022) and includes the use of ArUco markers (Garrido-Jurado et al., 2014) to continuously reconstruct the relative position of the cameras and overcome possible changes of camera orientation throughout experimental tests.

A bounding box automated detection routine was built using the Python library OpenCV (Bradski 2000) to capture the plastic samples contours and centre of gravity position per frame from the cameras video sequence (an exemplary routine is included in Lofty (2023)). The automated detection routine was composed of contrast-limited adaptive histogram equalization (CLAHE), to enhance contrast between the plastics and the background, and Gaussian blur techniques to diffuse small artefacts in the image. A background subtraction based on frame differencing was used to identify the moving plastics (see Fig. 1D for examples of the bounding box detection and supplementary videos for the automated detection routine).

The centre of gravity coordinates of the plastic samples was obtained per frame from the video sequence of two cameras, following a similar procedure as used in Huls (2022). Next, the plastic coordinates obtained from both cameras were then combined, considering the cross-camera time-synchronisation. In some instances, more than one sample was detected in the same video frame. To systematically classify the plastics detected in both camera recordings, a Gaussian mixture model (scikit library of Python (Pedregosa et al. 2011)) was used to match the individually detected plastic coordinates to a unique ID in both cameras. This methodology classifies plastic coordinates based on the plastic's time stamp and the horizontal position of the plastic's centre of gravity detected by each camera and is aided by a pre-processing routine in which the particle coordinates x_p-t_p, are used to find principal axes $x_p^{'}$-$t_p^{'}$ that assist in the unequivocal classification of particle trajectories. Based on the instantaneous position of the centre of gravity of each plastic by the two cameras, a 3D reconstruction was performed based on ray-crossing routines including refraction correction, based on methods by Duinmeijer et al. (2019) and as described in Valero et al. (2022).

3. Results and discussion

3.1. Multimodality of plastic settling

Through the 400 settling experiments, we identified that the settling velocities of the four negatively buoyant plastics were bimodally distributed, with all plastics exhibiting two main settling orientations, herein referred to as mode 1 (slower velocity w_{m1}, stable orientation) and mode 2 (faster velocity w_{m2}, metastable orientation). Each of these modes were identified through manual inspection of the video recordings of the settling experiments and based on both the geometrical configuration of the falling sample and its kinematics: oscillating or straight oblique settling (see supplementary videos for examples of the distinct settling orientation of the plastic samples).

Fig. 3A–D shows the settling velocity of each of the four tested plastic samples against the settling distance, relative to the water level, while Fig. 3E–H shows the histograms of the different modes of settling velocity for each plastic sample, as manually identified. For clarity, in Fig. 3 the two modes of settling are identified with different colours, and Table 3 shows the mean average settling velocity ($\overline{w}$, considering both modes), as well as the mean average for mode 1 (w_{m1}) and mean average for mode 2 (w_{m2}) settling velocity.

We hypothesize that a plastic-water system may be expected to reach a stable position when the mechanical energy is at a minimum. This can be mathematically written in terms of the mechanical energy derivative (relative to all variables) being zero and its second derivative being positive, as exemplified in Fig. 4. In analogy to equilibrium of a mechanical static system only dependent on potential energy, if a finite perturbation can move the system into a more strongly stable situation,

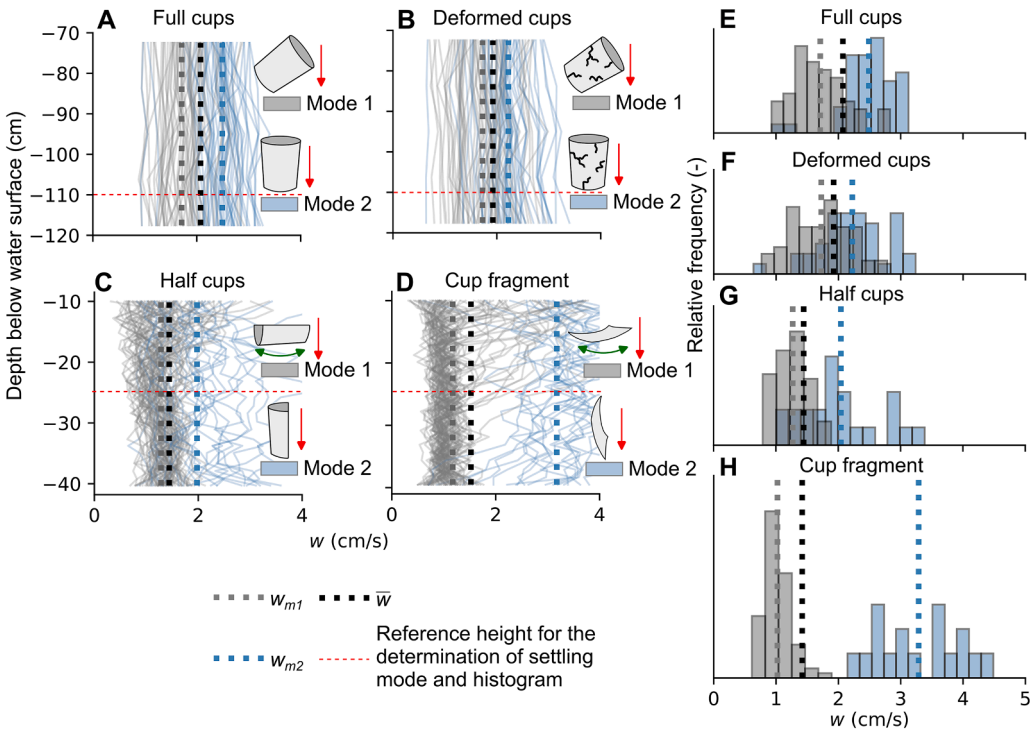

Fig. 3. Unique settling velocities and their histograms for each plastic sample. A-D) Settling velocities against the settling distance, relative to the water level for each plastic, coloured by settling mode (mode 1 and mode 2). E-H) Histograms of the settling velocities for each plastic taken at a vertical position of −110 cm for full and deformed cups and −25 cm for half cups and cup fragments, relative to the water level.

Table 3
Mean average settling velocity ($\overline{w}$) of the plastics samples. Average settling velocities of the samples used in experiments based on 100 settling tests per plastic sample, as well as mean mode 1 (w_{m1}) and mean mode 2 (w_{m2}) settling velocities. The percentage of samples which settled in either mode 1 or mode 2, at a vertical position of −110 cm for full and deformed cups and −25 cm for half cups and cup fragments, relative to the water level. The particle Reynolds number $\mathbf{Re_p}$ calculated as $\mathbf{Re_p} = wd_e/\nu$, corresponding to modes 1 (w_{m1}) and modes 2 (w_{m1}) of settling, where d_e represents the equivalent plastic diameter calculated as $d_e = \sqrt{4A/\pi}$ where A is the estimated projected horizontal area of the sample settling in an orientation corresponding to either mode 1 or mode 2.

Plastic	$\overline{w}$ (m/s)	w_{m1} (m/s)	w_{m2} (m/s)	% mode 1	% mode 2	$\mathbf{Re_p}$ (mode 1)	$\mathbf{Re_p}$ (mode 2)
Full cup	0.0207	0.0171	0.0249	60	40	1445	1793
Deformed cup	0.0192	0.0172	0.0222	54	46	1466	1599
Half cup	0.0145	0.0127	0.0204	78	22	1073	1040
Cup fragment	0.0142	0.0102	0.0329	80	20	548	671

then the original state is said to be metastable (and therefore the total energy was initially higher).

The mechanical energy of a plastic particle (E), also including the added water mass, at a reference elevation is the result of the contribution from kinetic energy (considering plastic mass and water virtual mass) and potential energy (related to the particle elevation and considering reduced gravity due to water immersion). For the sake of simplicity, we ignore rotational energy in the kinetic component. For a settling particle in a quiescent setting, if the horizonal velocity can be considered negligible in comparison to the vertical component, then the module of the particle velocity is approximately $\sim w$, and the total energy can be written as:

$$E \sim \frac{1}{2}\left(V_p\rho_p + V_{VM}\rho_w\right)w^2 + V_p\left(\rho_p - \rho_w\right)z_p \quad (3)$$

with z_p as the vertical position of the particle and the virtual mass corresponding to a volume V_{VM} with water density ρ_w, which is assumed to follow the settling velocity of the particle w. Approximate calculations (Table S1, Suppl. Material) suggest that, in our quiescent settling experiments, the kinetic energy associated to mode 1 is on average terms 79 % (from 34 % to 99 %) that of mode 2. This is however based on simplistic assumptions of the virtual mass (assumed as the projected frontal area times 1/3 of its equivalent diameter) and further research is needed for verification.

Therefore, at a given depth (i.e., equal potential energy component, z_p = constant):

- If more than one persistent settling velocity is observed, the lower settling velocity may commonly be expected to be more stable. This would be the case if the particle has minimal energy (driven by lower w^2, Eq. (3)), while the other settling state is metastable (Fig. 4). The reduction in mechanic energy of the lower w, however, could be compensated by an increase in the virtual mass volume (V_{VM} in Eq. (3)). With increasing w, a particle is observed to be more hydrodynamically aligned with the flow, therefore resulting in smaller wakes (i.e., reduction in V_{VM}). Our experimental observations (Fig. 3), nonetheless, suggest that the increase of w^2 compensates the reduction of V_{VM}, for the samples investigated, hence keeping the faster mode 2 altogether less stable.
- If an infinitely small perturbation (e.g., change of orientation) leads to a lower energy level (Eq. (3)), the original settling state can be classified as unstable (Fig. 4).

To further examine the particle orientation in both modes 1 and 2, in

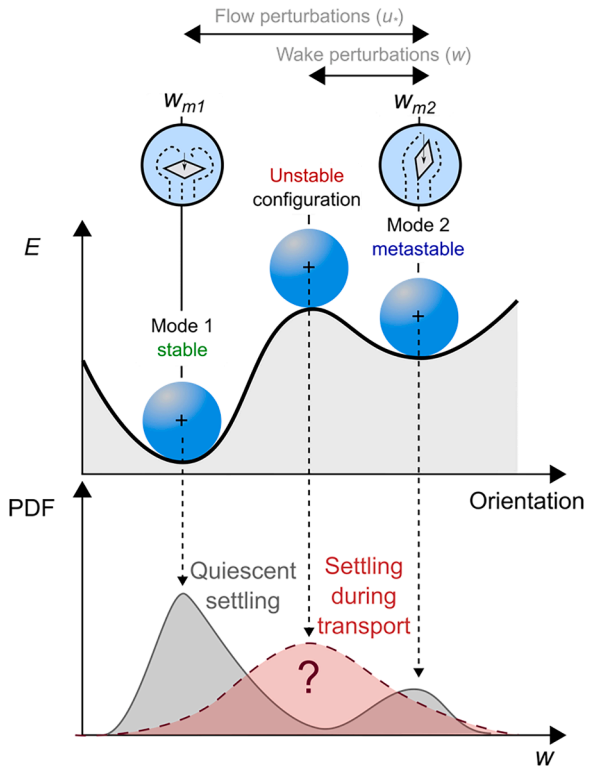

Fig. 4. Stability, metastability and instability in plastic settling. The relation between the mechanical energy of plastic particles and its degree of stability when settling; stable configuration (mode 1), metastable configuration (mode 2) and unstable configuration. Probability density function of the settling velocity of a plastic particle in a quiescent setting, and a hypothetical example of settling under transport conditions when plastic particles are subjected to turbulent forces strong enough to modify their falling orientation.

the following, we discuss the equilibrium quiescent settling velocity based on a simple balance of gravitational F_g and drag F_d forces, and assuming a dominant vertical motion, which requires:

$$F_g = F_d \tag{4}$$

$$(\rho_p - \rho_w) g V_p = \frac{1}{2} \rho_p C_d A w^2 \tag{5}$$

where C_d is the drag coefficient. Given that the immersed weight does not change across modes, we can write the following relationship between mode 1 and 2:

$$C_{d,1} A_{m,1} {w_{m,1}}^2 = C_{d,2} A_{m,2} {w_{m,2}}^2 \tag{6}$$

From the forces analysis, and regardless of the orientation of the settling particle, a settling mode with faster settling velocity needs to have a reduction of projected area (and thus wake) or drag coefficient (see Fig. S1 for specific changes in the drag coefficient) given by $C_{d,1}A_{m,1} / C_{d,2}A_{m,2} = {w_{m,2}}^2 / {w_{m,1}}^2$.

We observe in our experiments that mode 1 (slower settling velocity) is more predominant (i.e., stable), with largest exposed area $A_{m,1}$, while mode 2, the orientation reducing the virtual mass volume and the exposed area $A_{m,2}$, is less frequent (i.e., less stable). Interestingly, the ensembled average settling velocity ($\overline{w}$) is representative of a largely unobserved settling orientation with a velocity that was not often observed during experimental tests, which would correspond to an unstable or non-equilibrium settling configuration (Fig. 4), remaining in between stable and metastable states' settling velocities.

Due to their shape, full and deformed cups hold the smallest geometrical anisotropy of all the tested plastic samples, which can be explained by the inverse of the CSF (presented in Table 2). Given their heterogenous weight distribution, due to mass concentration in the base, cups tended to settle base-first, adopting either an angled orientation with a steady oblique trajectory (mode 1), or in an orientation with the base of the cup aligned normal to the predominant line of motion, corresponding to a faster metastable vertical settling trajectory (mode 2).

The probability of either mode of settling occurring for the full and deformed cups was relatively equal, provided that the initial drop angle was not enforced in a controlled position; 60 % of full cups and 54 % of deformed cups settled in the stable slower position mode 1 (Table 3). When considering the individual distribution functions of the full and deformed cups (mode 1 and mode 2), distributions tend to be symmetrical density functions (Fig. 3E). However, when combining the distributions of the full and deformed cups' mode 1 and mode 2 settling, a flatter –close-to-uniform– probability density function is observed for the settling velocities.

The half cups tended to settle in an orientation with their longest axis predominantly horizontal and concavity pointing upwards, in a slightly oscillating trajectory (mode 1), or a vertical orientation similar to the full and deformed cups (mode 2). In 78 % of the observations, half cups settled in mode 1 and this was the most stable settling orientation throughout the experiments (Table 3).

Conversely, the cup fragments correspond to a shape with the largest geometrical anisotropy of all the plastic samples. Cup fragments either settled with their broadest face (concavity upwards) normal to the predominant line of motion, in a slow oscillating oblique trajectory (mode 1), or in a faster vertical orientation, with their broadest face parallel to the predominant line of motion (mode 2). This represents the largest difference in settling modes investigated, and their falling dynamics corresponds to very different modes: mode 1 is governed by the form drag in the wake of the fragment while mode 2 shows a more streamlined drag, dominated by the developing boundary layer over the fragment's form (see supplementary videos). As a result, both modes have the most divergent distributions from the plastic samples, with 80 % of the cup fragments settling in mode 1 (Table 3). Initially, fragments could be settling in mode 2 and transition to the more stable position (mode 1) by rotation and remain stable for the remaining settling distance.

The findings here for the cup fragments are not consistent with previous theories on microplastic and sediment settling, which suggest that fragments (like films and foils) always settle with their broadest face (largest projected area) normal to the predominant line of motion (Wadell 1932; Rubey 1933; Corey et al., 1949; Goral et al. 2023). Our observations support the coexistence of multiple (stable and metastable) modes of settling for macroplastics, on the basis of Eqs. (3) and (4), each with distinct settling velocities and wake regions. The difference between these settling velocities increases with greater geometrical anisotropy because of differences in exposed areas described by Eq. (6), while the slower and more stable settling mode (mode 1) becomes more frequent with decreasing w_{m2}/w_{m1} ratios in our experiments. This insight has been previously observed for many different anisotropic shapes including disks, cards and cylinders of different densities (Andersen et al., 2005; Ern et al., 2012; Auguste et al., 2013; Voth and Soldati 2017), but has yet to be applied within the context of plastic pollution transport.

3.2. *Three-dimensional plastic trajectories in transport and vertical distribution of plastics*

During the transport experiments, samples were transported by the flow and were vertically distributed by turbulence through the water column (Fig. 5). When the plastics moved into the observation window , they were detected by a synchronous multi-camera system. The detected plastics can be transported within three different layers, based on their vertical position in the observation window:

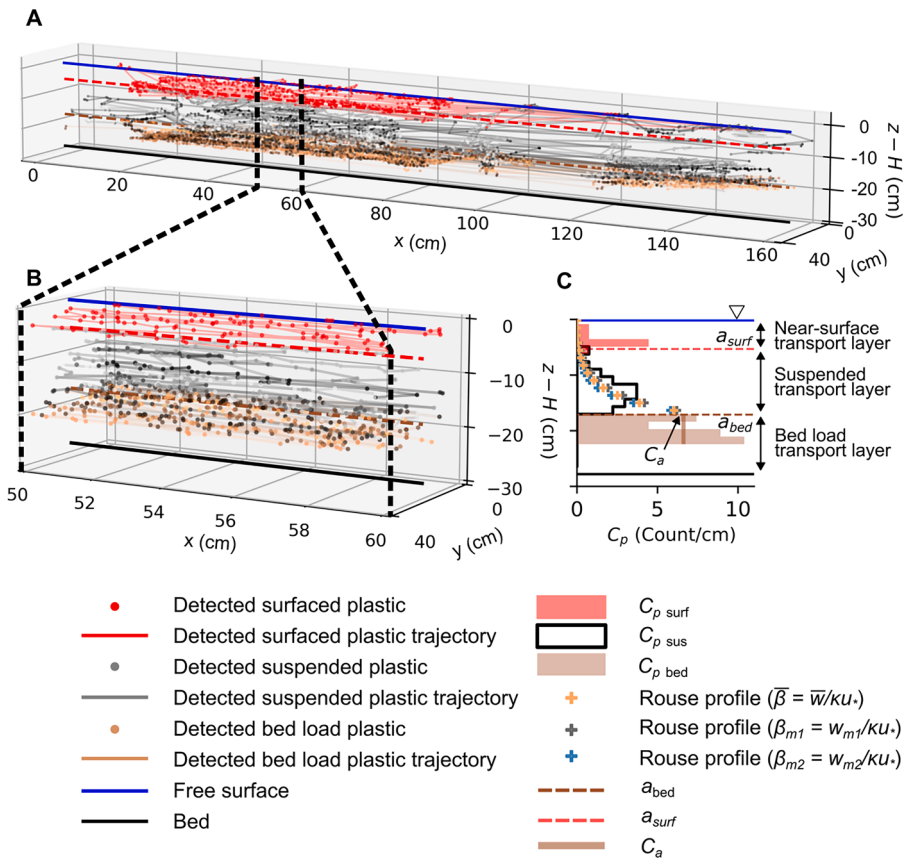

Fig. 5. 3D plastic trajectories and corresponding vertical concentration profile obtained from experiments. A) An example of ~150 deformed cup plastic trajectories moving through the observation window ($x = 0$ to 100 cm) and beyond at $u_* = 0.0213$ m/s (i.e., range of $\overline{\beta}$, β_{m1} and β_{m2} values = 1.99 – 2.23) detected by synchronous multi-camera detection and 3D reconstructed. B) The analysis section at $x = 50$ to 60 cm within the observation window at which best available trajectories were captured for vertical concentration profiles. C) The vertical concentration profile for the half cups corresponding to the 3D trajectories shown in Fig. 5B, displaying three Rouse concentration profiles based on $\overline{\beta}$, β_{m1} and β_{m2}. $x = 0$ corresponds to the start of the observation window at 10.62 m from the insertion point of plastics.

1. The *near-surface layer* (coloured in red in Fig. 5) defined as plastics in contact with the free surface or in the near-surface region, confined to a layer $a_{surf} = 0.5\lambda$ (λ, maximum diagonal length of a particle, Table 2 in thickness as described in Valero et al. (2022) where transport is expected to be driven by the balance between the relative settling/rising velocity of a particle, surface tension (when in contact with the surface) and turbulence.
2. The *bed load layer* (coloured in brown in Fig. 5) defined by the occurrence of plastics in frequent contact with the bed or in the near-bed region at a distance $a_{bed} = \lambda$, based on definitions for sediment load concentration profiles (Einstein 1950; Garcia 2008). Transport in this layer is expected to be driven by the balance of the relative settling/rising velocity of a particle, turbulence, lift and particle-bed interactions (van Rijn 1984; Lofty et al., 2023b).
3. The *suspended transport layer* (coloured in grey in Fig. 5), which is defined as the layer between the near-surface and bed load layers and where transport of plastics is expected to be driven by the balance of the relative settling/rising velocity of a particle and turbulence.

Fig. 5A shows an example of ~150 deformed cup trajectories, moving through the observation window (and beyond), for $u_* = 0.0213$ m/s ($U = 0.318$ m/s), with Fig. 5B showing the section at $x = 50$ to 60 cm in which plastics were detected more consistently across the whole observation window; i.e., no visual obstruction from ArUco markers and flume superstructure, and therefore considered for the composition of the vertical concentration profiles of plastics. Fig. 5C depicts the vertical concentration profile corresponding to the same deformed cup plastic trajectories with a bin size of 0.25λ, divided into surface ($C_{p\ surf}$), suspended ($C_{p\ sus}$) and bed load layers ($C_{p\ bed}$).

Three theoretical suspended concentration profiles, based on the Rouse profile (Eq. (2)) (Rouse 1939), are also plotted in Fig. 5C based on three different Rouse numbers β (Eq. (1)), calculated based on the physical parameters; the settling velocities of the plastic samples $\overline{w}$, w_{m1} and w_{m2} (Table 3) and the shear velocity of the flow u_*. Specifically, these three Rouse profiles correspond to:

1. a profile based on $\overline{\beta}$ calculated with $\overline{w}$ i.e. $\overline{\beta} = \overline{w}/\kappa u_*$,
2. a profile based on β_{m1} (settling mode 1) calculated with w_{m1} i.e. $\beta_{m1} = w_{m1}/\kappa u_*$,
3. and a profile based on β_{m2} (settling mode 2) calculated with w_{m2} i.e. $\beta_{m2} = w_{m2}/\kappa u_*$.

The range of β values used in the Rouse suspended concentration

Table 4
Range of Rouse numbers β for the plastic samples considering $\overline{\beta}$, β_{m1} and β_{m2}, which are based on the average settling velocity ($\overline{w}$) and the different modes of setting and their corresponding velocities (w_{m1} and w_{m2}) (Table 3), as well as the five flow conditions used in experiments.

Plastic	Range of $\overline{\beta}$	Range of β_{m1}	Range of β_{m2}
Full cup	0.83 – 2.37	0.68 – 1.96	0.99 – 2.85
Deformed cup	0.77 – 2.20	0.68 – 1.97	0.88 – 2.54
Half cup	0.58 – 1.10	0.51 – 0.97	0.81 – 1.55
Cup fragment	0.65 – 1.62	0.41 – 1.17	1.31 – 3.76

profiles across all experiments are also shown in Table 4 for all flow conditions, showing that the performed experiments cover bed load ($7.5 > \beta > 2.5$), suspended load ($2.5 > \beta > 0.8$), and wash load ($0.8 > \beta > 0$), transport dynamics (Dey 2014).

The reference concentration C_a used in Eq. (2) is defined as the average concentration of detected plastics within the bed load transport layer (number of bed load plastic divided by the observed bed load layer thickness). The reference height a is defined as a_{bed}, corresponding to the demarcation line between bed load and suspended load transport as earlier defined. The vertical concentration profiles and Rouse profiles for all plastics and flow conditions tested are presented in Fig. S2.

The vertical concentration profiles show, as expected, that the vertical distribution of plastics with slower settling velocities are more susceptible to turbulence (i.e., cases with smaller β), which imply that plastics were observed more frequently in the suspended and near-surface layers of the water column. Conversely, the vertical distribution of plastics with a faster settling velocity, are less susceptible to turbulent transport, hence transport is influenced more by gravitational forces and plastics were observed more frequently closer to the bed (as per larger β). Regardless of being negatively buoyant, the plastic samples were observed to overconcentrate in the near-surface layers, mostly due to the surface tension effect, which is strong enough to hold the plastics captive by the free surface against turbulence and their submerged weight, similar to results by Valero et al. (2022) for positively buoyant plastic.

Interactions between near-surface, suspended and bed load layers were observed. For instance, following an impact with the channel bed, some plastic samples migrated from the bed layer directly to the suspended layers and even to the free surface. The migration of plastics from bed to near-surface layers due to particle-bed impacts could be associated to the spin generated in the bed impact, which induces lift forces, promoting vertical transportation of plastics (see supplementary videos).

Plastic particle-bed rebound kinematics are expected within the bed load layers at β values studied in this experiment (Table 4). According to the study by Lofty et al. (2023b), under the assumption of spherical plastics, the average saltation height of a plastic after impact with the bed, H_p, can be estimated by $H_p/L_{\max} = 4.236\beta^{-0.593}$. For the experiments conducted, a full cup transported in the bed load layers would be expected to saltate, on average terms, to a height of 0.18 – 0.42 m and, therefore, potentially up to the free surface during these experiments. The estimation of the saltation height considering such further theoretical approaches such as van Rijn (1984) and Lee et al. (2000), developed for the saltation characteristics of mineral sediments in bed load, require detailed knowledge on incipient motion of the plastic that are not available in this study; however, an order of magnitude analysis shows that this bed load-to-surface layer migration theory is consistent. We note that the size of the plastics used in this experiment (Table 2) is considerably large in comparison with the water depth (Table 1). In large rivers, this may be different, in particular the frequency of bed load to near surface migration.

Altogether, two distinct mechanisms are observed for transporting negatively buoyant plastics to the surface layer, where surface tension can retain plastics against their apparent weight: i) turbulence and ii) particle-bed rebound kinematics, with the latter potentially becoming less frequent as the water depth increases (or the particle size decreases).

3.3. Vertical concentration profiles of plastics and applicability of the Rouse profile

Vertical concentration profiles for suspended particles such as the theoretical Rouse concentration profile (Rouse 1939), can be used as predictive models for gauging the concentration of plastics within the suspended transport region (Fig. 5C). Such vertical concentration profiles can be drawn from sampling plastics in a river at a given depth (Cowger et al., 2021) and allows more accurate plastic budget predictions (Valero et al., 2022); however, their adequacy and limitations are yet to be examined.

To assess the applicability of the Rouse profile (Eq. (2)) as a vertical concentration profile to describe plastics in the suspended layers, we investigate the potential differences between the cumulative probability distributions (CDFs) of the particle positions obtained in the experiments from the suspended and near-surface layers and the normalised cumulative distributions of three Rouse profiles calculated based on $\overline{\beta}$, β_{m1} and β_{m2}. Comparing CDFs is more appropriate than comparing probability distribution functions (PDFs) (e.g., a concentration profile as seen in Figs. 5C and S2) as the interpretation of PDFs can be subjective due to the bin-size dependence (Wilks 2006). When comparing CDFs, a measure of the similarity between distributions (i.e., the experimental CDF, $F_0(z)$, and the normalised CDF of the theoretical Rouse profiles, $F_r(z)$) can be calculated via the Kolmogorov-Smirnov (KS) distance (D):

$$D = \text{Max}\ (z)|F_0(z) - F_r(z)| \tag{7}$$

Fig. 6 shows the CDFs for all the plastic samples and Rouse profiles (considering $\overline{\beta}$, β_{m1} and β_{m2}) for all flow conditions, while Fig. 7 shows the KS distance values against the range of β ($\overline{\beta}$, β_{m1} and β_{m2}) values determined from all experiments.

Figs. 6 and 7 show that, for higher values of β, the observed CDFs for the plastic samples become more inconsistent with the theoretical Rouse profiles (considering all the Rouse integrals calculated by $\overline{\beta}$, β_{m1} and β_{m2}). Visually, we observe that for higher values of β, the vertical concentration profiles tend to adhere to a more uniform distribution throughout the water column. This represents, for higher values of β, more vertically dispersion in the mass transfer than anticipated through the Rouse theory.

The discrepancies between the observed profiles and the Rouse profiles shown in Figs. 6 and 7 may be caused by more frequent particle-bed interactions at higher values of β, where the relative importance of gravitational forces is greater. These particle-bed interactions were seen to facilitate the migration of plastics from the bed load layer to the suspended and near-surface layers, as presented in Section 3.2. This process enhances mixing beyond what the Rouse profile (i.e., solely the balance between settling and turbulence) can explain, resulting in concentration profiles that display greater uniformity at higher β values. This leads to an increase in error for the Rouse profiles. However, as turbulence increases, particle-bed impact dynamics are less dominant and plastics remain more in the suspended and near-surface layers, thus resulting in CDFs becoming more consistent with the Rouse integrals (Fig. 7).

As a result, it is observed that the bed load layer thickness (a_{bed}) for the plastic samples stretches up to 1.5 – 2 λ (based on deviations observed in Fig. 6), which is significantly larger in absolute terms than bed load thickness definitions for sediment transport (Einstein 1950; Garcia 2008). This renders bed load dynamics as more influential in the transport of plastic across a larger region of the water column when compared to near-surface dynamics.

At lower β values, where particles remain in the suspended and near-surface layers of the water column, it is observed that a Rouse integral that is based on the ensembled average settling velocity, calculated in during the settling experiments i.e. $\overline{\beta} = \overline{w}/\kappa u_*$, reduced the error in predicting the particle's vertical concentration profile for all particles, compared to Rouse integrals based on β_{m1} and β_{m2} (Figs. 6 and 7). Although samples displayed distinct stable (and metastable) orientations during quiescent settling, these same settling states and behaviours are not exhibited while the particle was in turbulent flow, which increases error when predicting vertical concentration profiles with β_{m1} and β_{m2}. This is because during quiescent settling, the wake of the particle is solely responsible for perturbations that can change the orientation of the particle (roughly, perturbations up to 30 % of the modal settling velocity, based on previous particle-wake studies (Ern et al.,

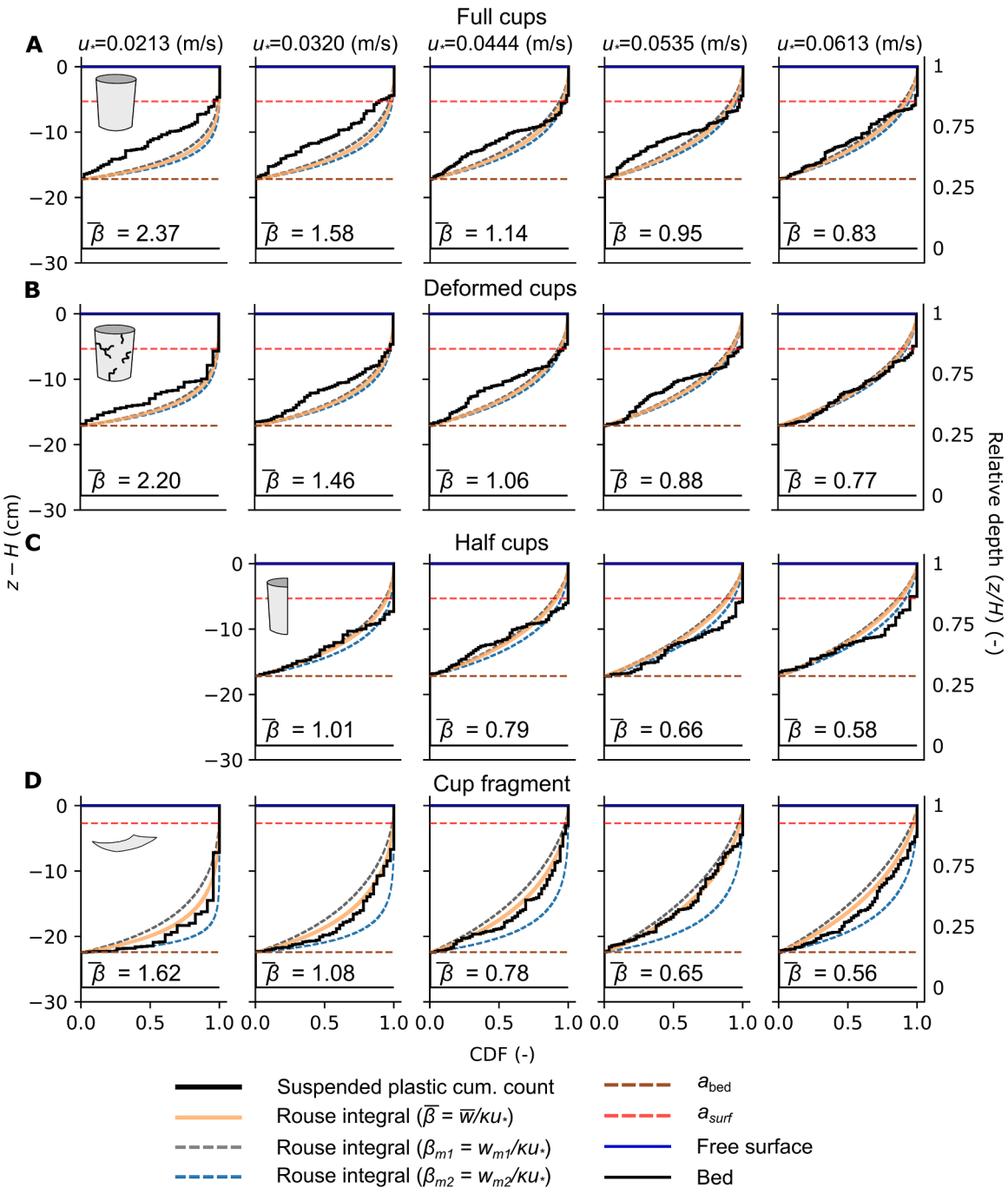

Fig. 6. CDFs of the vertical positions of the plastics obtained in the experiments from the near-surface and suspended transport layers, as well as the normalised cumulative distributions of three Rouse prof calculated based by $\overline{\beta}$, β_{m1} and β_{m2} for the A) full cups, B) deformed cups, C) half cups and D) cup fragments, across all the flow conditions tested.

2012)). However, in river-like turbulent flows, inner-wall turbulence can commonly produce perturbations in the order of magnitude of u_* (Pope 2000), or even two to three times larger in very intense eddies. This may trigger new stable (or metastable) plastic-orientations, with a frequency for each orientation during turbulent settling that is different from quiescent settling (Voth and Soldati 2017; Baker and Coletti 2022) (Fig. 4). As a result, vertical concentration profiles can still be determined, within experimental uncertainty, by mean settling velocity $\overline{w}$ of a plastic particle.

4. Conclusion

Two mechanisms that affect the transport of plastics are studied in this investigation. The first relates to the development of complex, multimodal settling configurations. While one mode tends to be more stable than other modes, these other modes can be metastable and present very different velocities, roughly satisfying $C_{d,1}A_{m,1}{w_{m,1}}^2 = C_{d,2}A_{m,2}{w_{m,2}}^2$. During quiescent settling, the wake of the particle is solely responsible for the perturbations that can change the orientation of the particle. However, during the transport in a boundary layer flow as in river flows (Franca et al., 2022), inner-wall turbulence may produce perturbations that are large enough to trigger new

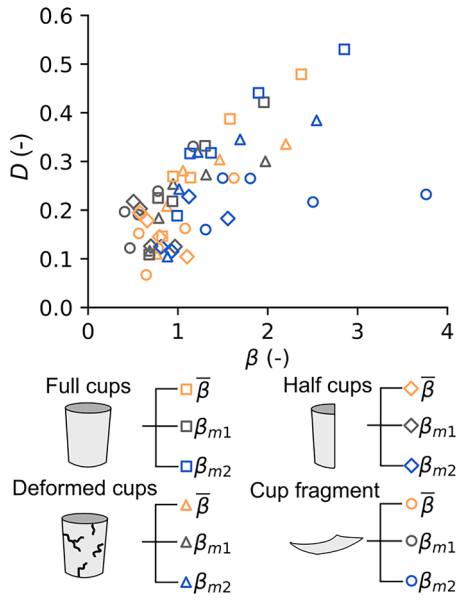

Fig. 7. KS distance (D) values calculated through Eq. (7) against the range of β values determined from experiments (considering $\overline{\beta}$, β_{m1} and β_{m2}).

plastic-orientations, with a frequency for each orientation during turbulent settling that is different from quiescent settling (Fig. 4).

From a stochastic perspective of transport, the settling velocity has a probability density distribution ($p(w)$), leading to a weighted average for the concentration distribution at a given depth z:

$$C(z) = \int \left(C_a \left[\left(\frac{H-z}{z} \right) \left(\frac{a}{H-a} \right) \right]^{\beta} \right) \cdot p(w) \mathrm{d}w \tag{8}$$

From a more pragmatic perspective, within the uncertainty of our results, deterministic calculations can still be performed on the basis of the ensemble average settling velocity (but not the median, given settling bimodality), as suggested in Figs. 6 and 7. Therefore, a set of settling experiments needs to be conducted to estimate $\overline{w}$ through an ensemble average, but bimodality (or in general multimodality) increases the variance and therefore requires a larger number of experiments (N) to reach an acceptable level of uncertainty. Taking, as reference, the 100 settling experiments conducted herein for each plastic sample, we observe that in order to keep uncertainty for $\overline{w}$ below 10 %, a minimum $N = 15$ is required (see Fig. S3).

The second mechanism observed in this investigation is the interaction of plastics with the channel bed and the extent at which it affects vertical concentration profiles across the water column. Particle-bed impacts induces differences in vertical concentration distributions across a large region (1.5 – 2 λ, Fig. 6), not only in the near-bed region, as opposed to the near-surface dynamics (0.5λ), which have a more localized effect (Valero et al., 2022). For the higher β values examined, this mechanism has a deeper impact on the vertical transport of plastics than multimodality in settling.

5. Associated content

5.1. Supporting information

Fig. S1. Drag coefficient $C_d$and Particle Reynolds number Re_P relationship for particles settling in modes 1 and modes 2.

Fig. S2. The vertical concentration profiles, with bin size = 0.25λ, and Rouse profiles calculated by $\overline{\beta}$, β_{m1} and β_{m2}.

Fig. S3. Error in sampling settling velocities.

Table S1. Approximate kinetic energy levels (KE, based on the mechanical energy of Eq. (3) with $z_p = 0$ m) for the two settling modes of each particle identified in the settling tanks. The virtual mass is approximated as the projected frontal area of each particle times 1/3 of its equivalent diameter.

Movie S1. Mode 1 of settling in a quiescent experiment for a half cup.

Movie S2. Mode 2 of settling in a quiescent experiment for a half cup.

Movie S3. Mode 1 of settling in a quiescent experiment for a cup fragment.

Movie S4. Mode 2 of settling in a quiescent experiment for a cup fragment.

Movie S5. Mode 1 of settling in a quiescent experiment for a full cup.

Movie S6. Mode 2 of settling in a quiescent experiment for a full cup.

Movie S7. Exemplary transfer of bed load particle to upper layer of the flow after a bed-particle interaction.

Movie S8. Automated particle detection example.

Corresponding Author
† James Lofty: LoftyJ@cardiff.ac.uk
* Daniel Valero: d.valero@imperial.ac.uk

Funding sources

The UK Engineering and Physical Sciences Research Council (EPSRC) Grant number EP/T517951/1 (CW & JL).

Erasmus+ 2023 mobility programme (JL). Karlsuhe House of Young Scientists Mobility grant (JL & DV)

Dutch Ministry of Foreign Affairs, Orange Knowledge Programme (OKP), Grant number: OKP-MA.19/00,395 (BB)

Dutch Ministry of Infrastructure and Water Management (Rijkswaterstaat), under MoU scheme with IHE Delft (DV)

Data and codes availability

Processed data and relevant codes are available under: https://github.com/JamesLofty/suspended_macroplastic

CRediT authorship contribution statement

James Lofty: Conceptualization, Data curation, Investigation, Visualization, Writing – original draft, Writing – review & editing. **Daniel Valero:** Conceptualization, Investigation, Methodology, Supervision, Visualization, Writing – original draft, Writing – review & editing. **Antonio Moreno-Rodenas:** Methodology, Writing – review & editing. **Biruk S. Belay:** Methodology. **Catherine Wilson:** Supervision, Writing – review & editing. **Pablo Ouro:** Supervision, Writing – review & editing. **Mário J. Franca:** Conceptualization, Supervision, Writing – review & editing.

Declaration of competing interest

The authors declare that they have no known competing financial interests or personal relationships that could have appeared to influence the work reported in this paper.

Data availability

Data will be made available on request.

Supplementary materials

Supplementary material associated with this article can be found, in the online version, at doi:10.1016/j.watres.2024.121306.

References

Amereh, F., et al., 2022. Placental plastics in young women from general population correlate with reduced foetal growth in IUGR pregnancies. Environ. Pollut. 314,

120174. Available at: https://linkinghub.elsevier.com/retrieve/pii/S0269749122013884.
Andersen, A., Pesavento, U., Wang, Z.J., 2005. Analysis of transitions between fluttering, tumbling and steady descent of falling cards. J. Fluid. Mech. 541 (1), 91. Available at: http://www.journals.cambridge.org/abstract_S0022112005005847.
Auguste, F., Magnaudet, J., Fabre, D., 2013. Falling styles of disks. J. Fluid. Mech. 719, 388–405. Available at. https://www.cambridge.org/core/product/identifier/S0022112012006027/type/journal_article.
Baker, L.J., Coletti, F., 2021. Particle–fluid–wall interaction of inertial spherical particles in a turbulent boundary layer. J. Fluid. Mech. 908, p. A39. Available at. https://www.cambridge.org/core/product/identifier/S0022112020009349/type/journal_article.
Baker, L.J., Coletti, F., 2022. Experimental investigation of inertial fibres and disks in a turbulent boundary layer. J. Fluid. Mech. 943, A27. Available at: https://www.cambridge.org/core/journals/journal-of-fluid-mechanics/article/experimental-investigation-of-inertial-fibres-and-disks-in-a-turbulent-boundary-layer/0261D874F98C7C0981D1B06ACB8223DD.
Bergmann, M., et al., 2022. A global plastic treaty must cap production. Science 376 (6592), 469–470 (1979)Available at. https://www.science.org/doi/10.1126/science.abq0082.
Blanckaert, K. and Lemmin, U. 2010. Means of noise reduction in acoustic turbulence measurements. https://doi.org/10.1080/00221686.2006.9521657 44(1), pp. 3–17. Available at: https://www.tandfonline.com/doi/abs/10.1080/00221686.2006.9521657.
Blondel, E., Buschman, F.A., 2022. Vertical and horizontal plastic litter distribution in a bend of a tidal river. Front. Environ. Sci. 10. Available at: https://www.frontiersin.org/articles/10.3389/fenvs.2022.861457/full.
Born, M.P., Brüll, C., Schaefer, D., Hillebrand, G., Schüttrumpf, H., 2023. Determination of Microplastics' vertical concentration transport (Rouse) profiles in flumes. Environ. Sci. Technol. 57 (14), 5569–5579. Available at: https://pubs.acs.org/doi/10.1021/acs.est.2c06885.
Bradski, G. 2000. The openCV library. Dr. Dobb's Journal: Software Tools for the Professional Programmer 25(11), pp. 120–123.
Christiansen, E.B., Barker, D.H., 1965. The effect of shape and density on the free settling of particles at high Reynolds numbers. AIChE J. 11 (1), 145–151. Available at: https://onlinelibrary.wiley.com/doi/10.1002/aic.690110130.
Clark, B.L., et al., 2023. Global assessment of marine plastic exposure risk for oceanic birds. Nat. Commun. 14 (1), 1–14, 2023 14:1Available at: https://www.nature.com/articles/s41467-023-38900-z.
Corey, A.T., Albertson, M.L., Fults, J.L., Rollins, R.L., Gardner, R.A., Klinger, B. and Bock, R.O. 1949. Influence of shape on the fall velocity of sand grains. Available at: https://mountainscholar.org/handle/10217/195976.
Cowger, W., Gray, A.B., Guilinger, J.J., Fong, B., Waldschläger, K., 2021. Concentration depth profiles of microplastic particles in river flow and implications for surface sampling. Environ. Sci. Technol. 55 (9), 6032–6041. Available at: https://pubs.acs.org/doi/full/10.1021/acs.est.1c01768.
De-la-Torre, G.E., 2020. Microplastics: an emerging threat to food security and human health. J. Food Sci. Technol. 57 (5), 1601–1608. Available at: https://pubmed.ncbi.nlm.nih.gov/32327770/.
Dey, S., 2014. Fluvial Hydrodynamics. Springer Berlin Heidelberg, Berlin, Heidelberg. https://doi.org/10.1007/978-3-642-19062-9.
Duinmeijer, S.P.A., Moreno-Rodenas, A.M., Lepot, M., van Nieuwenhuizen, C., Meyer, I., Clemens, F.H.L.R., 2019. A simple measuring set-up for the experimental determination of the dynamics of a large particle in the 3D velocity field around a free surface vortex. Flow Meas. Instrum. 65, 52–64. https://doi.org/10.1016/j.flowmeasinst.2018.10.007.
Einstein, H.A. 1950. The bed-load function for sediment transportation in open channel flows. Available at: https://ageconsearch.umn.edu/record/156389.
Elata, C., Ippen, A.T., 1961. The Dynamics of Open Channel Flow With Suspensions of Neutrally Buoyant particles. Hydrodynamic Laboratory Technical Report No. 45. Cambridge.
Ern, P., Risso, F., Fabre, D., Magnaudet, J., 2012. Wake-induced oscillatory paths of bodies freely rising or falling in fluids. Annu Rev. Fluid. Mech. 44 (1), 97–121. Available at: https://www.annualreviews.org/doi/10.1146/annurev-fluid-120710-101250.
Field, S.B., Klaus, M., Moore, M.G., Nori, F., 1997. Chaotic dynamics of falling disks. Nature 388 (6639), 252–254. Available at: https://www.nature.com/articles/40817.
Franca, M.J., Valero, D., Liu, X., 2022. Turbulence and rivers. Treatise On Geomorphology. Elsevier, pp. 151–175. Available at: https://linkinghub.elsevier.com/retrieve/pii/B9780128182345001358.
Garcia, M., 2008. Sedimentation Engineering. Garcia, M. American Society of Civil Engineers, Reston, VA. Available at: https://ascelibrary.org/doi/book/10.1061/9780784408148.
Garrido-Jurado, S., Muñoz-Salinas, R., Madrid-Cuevas, F.J., Marín-Jiménez, M.J., 2014. Automatic generation and detection of highly reliable fiducial markers under occlusion. Pattern. Recognit. 47 (6), 2280–2292. https://doi.org/10.1016/j.patcog.2014.01.005.
Geraeds, M., van Emmerik, T., de Vries, R., bin Ab Razak, M.S., 2019. Riverine plastic litter monitoring using unmanned aerial vehicles (UAVs). Remote Sens. 11 (17), 2045, 2019, Vol. 11, Page 2045Available at: https://www.mdpi.com/2072-4292/11/17/2045/htm.
Geyer, R., Jambeck, J.R., Law, K.L., 2017. Production, use, and fate of all plastics ever made. Sci. Adv. 3 (7) p. e1700782. Available at. https://www.ncbi.nlm.nih.gov/pubmed/28776036.
González-Fernández, D., Hanke, G., 2017. Toward a harmonized approach for monitoring of riverine floating macro litter inputs to the marine environment. Front. Mar. Sci. 245955. https://doi.org/10.3389/fmars.2017.00086/full.
Goral, K.D., et al., 2023. Settling velocity of microplastic particles having regular and irregular shapes. Environ. Res. 228, 115783. Available at: https://linkinghub.elsevier.com/retrieve/pii/S0013935123005753.
Hartmann, N.B., Hüffer, T., Thompson, R.C., Hassellöv, M., Verschoor, A., Daugaard, A.E., Rist, S., Karlsson, T., Brennholt, N., Cole, M., Herrling, M.P., Hess, M.C., Ivleva, N.P., Lusher, A.L., Wagner, M., 2019. Are We Speaking the Same Language? Recommendations for a Definition and Categorization Framework for Plastic Debris. Environ. Sci. Technol. 53 (3), 1039–1047. https://doi.org/10.1021/acs.est.8b05297.
Huls, M. 2022. Detecting Motion with OpenCV — image analysis for beginners | by Mike Huls | Towards Data Science. Available at: https://towardsdatascience.com/image-analysis-for-beginners-creating-a-motion-detector-with-opencv-4ca6faba4b42.
Hurley, R., et al., 2023. Measuring riverine macroplastic: methods, harmonisation, and quality control. Water Res. 235, 119902. Available at: https://linkinghub.elsevier.com/retrieve/pii/S004313542300338X.
ISO 2019. ISO 1183-1:2019 - Plastics — Methods for determining the density of non-cellular plastics — Part 1: Immersion method, liquid pycnometer method and titration method. Available at: https://www.iso.org/standard/74990.html.
Jayaweera, K.O.L.F., Mason, B.J., 1965. The behaviour of freely falling cylinders and cones in a viscous fluid. J. Fluid. Mech. 22 (04), 709. Available at: http://www.journals.cambridge.org/abstract_S002211206500109X.
Jenner, L.C., Rotchell, J.M., Bennett, R.T., Cowen, M., Tentzeris, V., Sadofsky, L.R., 2022. Detection of microplastics in human lung tissue using μFTIR spectroscopy. Sci. Total Environ. 831, 154907.
Kaftori, D., Hetsroni, G., Banerjee, S., 1995. Particle behavior in the turbulent boundary layer. II. Velocity and distribution profiles. Phys. Fluids 7 (5), 1107–1121. Available at: https://pubs.aip.org/pof/article/7/5/1107/259535/Particle-behavior-in-the-turbulent-boundary-layer.
Kataoka, T., Nihei, Y., 2020. Quantification of floating riverine macro-debris transport using an image processing approach. Sci. Rep. 10 (1), 1–11, 2020 10:1Available at: https://www.nature.com/articles/s41598-020-59201-1.
Kuizenga, B., Van Emmerik, T., Waldschläger, K., Kooi, M., 2022. Will it float? Rising and settling velocities of common macroplastic foils. ACS ES T Water 2 (6), 975–981. https://doi.org/10.1021/ACSESTWATER.1C00467.
Lee, H.Y., Chen, Y.H., You, J.Y., Lin, Y.T., 2000. Investigations of continuous bed load saltating process. J. Hydraul. Eng. 126 (9), 691–700. https://doi.org/10.1061/(asce)0733-9429(2000)126:9(691).
Leslie, H.A., van Velzen, M.J.M., Brandsma, S.H., Vethaak, A.D., Garcia-Vallejo, J.J., Lamoree, M.H., 2022. Discovery and quantification of plastic particle pollution in human blood. Environ. Int. 163, 107199 https://doi.org/10.1016/J.ENVINT.2022.107199.
Lofty, J., Ouro, P., Wilson, C.A.M.E., 2023a. Microplastics in the riverine environment: meta-analysis and quality criteria for developing robust field sampling procedures. Sci. Total Environ. 863, 160893. Available at: https://linkinghub.elsevier.com/retrieve/pii/S0048969722079967.
Lofty, J., Valero, D., Wilson, C.A.M.E., Franca, M.J., Ouro, P., 2023b. Microplastic and natural sediment in bed load saltation: material does not dictate the fate. Water Res. 243, 120329. Available at: https://linkinghub.elsevier.com/retrieve/pii/S0043135423007650.
Lofty, J. 2023. JamesLofty/suspended_macroplastic: suspended_macroplastic_1. Available at: https://zenodo.org/record/8321370.
MacLeod, M., Arp, H.P.H., Tekman, M.B., Jahnke, A., 2021. The global threat from plastic pollution. Science 373 (6550), 61–65 (1979)Available at: https://www.science.org/doi/10.1126/science.abg5433.
McGoran, A.R., Clark, P.F., Smith, B.D., Morritt, D., 2023. Macrolitter and mesolitter in the Thames Estuary: a temporal litter assessment and brand audit of submerged and riverbed debris. Environ. Pollut. 337, 122484. Available at: https://linkinghub.elsevier.com/retrieve/pii/S0269749123014860.
Muste, M., Yu, K., Fujita, I., Ettema, R., 2005. Two-phase versus mixed-flow perspective on suspended sediment transport in turbulent channel flows. Water Resour. Res. 41 (10) https://doi.org/10.1029/2004WR003595.
Nguyen, K.L.P., Bui, T.K.L., 2023. Riverbank macro-litters monitoring in downstream of Saigon river, Ho Chi Minh City. Case Stud. Chem. Environ. Eng. 7, 100306 https://doi.org/10.1016/J.CSCEE.2023.100306.
Pedregosa, F., et al., 2011. Scikit-learn: machine learning in Python. J. Mach. Learn. Res. 12, 2825–2830.
Pope, S.B. 2000. Turbulent Flows. Available at: https://www.cambridge.org/core/product/identifier/9780511840531/type/book.
Ragusa, A., et al., 2022. Deeply in Plasticenta: presence of microplastics in the intracellular compartment of human placentas. Int. J. Environ. Res. Public Health 19 (18). Available at. https://pubmed.ncbi.nlm.nih.gov/36141864/.
Rashidi, M., Hetsroni, G., Banerjee, S., 1990. Particle-turbulence interaction in a boundary layer. Int. J. Multiph. Flow 16 (6), 935–949. Available at: https://linkinghub.elsevier.com/retrieve/pii/0301932290900995.
Rouse, H. 1939. An analysis of sediment transportation in the light of fluid turbulence. Available at: https://resolver.caltech.edu/CaltechAUTHORS.
Rubey, W.W., 1933. Settling velocity of gravel, sand, and silt particles. Am. J. Sci. s5-25 (148), 325–338. Available at. https://www.ajsonline.org/content/s5-25/148/325.
Russell, C.E., Fernández, R., Parsons, D.R., Gabbott, S.E., 2023. Plastic pollution in riverbeds fundamentally affects natural sand transport processes. Commun. Earth Environ. 4 (1), 1–10, 2023 4:1Available at: https://www.nature.com/articles/s43247-023-00820-7.

UNEP, 2021. From Pollution to Solution: a global assessment of marine litter and plastic pollution. Nairobi. Available at: https://www.unep.org/resources/pollution-solution-global-assessment-marine-litter-and-plastic-pollution.

UNEP UNEA Resolution 5/14 Entitled "End Plastic pollution: Towards an International Legally Binding Instrument, 2023. United Nations Environment Programme, Dakar, Senegal.

Valero, D., Belay, B.S., Moreno-Rodenas, A., Kramer, M., Franca, M.J., 2022. The key role of surface tension in the transport and quantification of plastic pollution in rivers. Water Res. 226, 119078 https://doi.org/10.1016/j.watres.2022.119078.

van Emmerik, T., Schwarz, A., 2020. Plastic debris in rivers. WIREs Water 7 (1). Available at. https://onlinelibrary.wiley.com/doi/10.1002/wat2.1398.

van Emmerik, T., et al., 2018. A methodology to characterize riverine macroplastic emission into the ocean. Front. Mar. Sci. 5. Available at: https://www.frontiersin.org/articles/10.3389/fmars.2018.00372/full.

van Emmerik, T., Roebroek, C., De Winter, W., Vriend, P., Boonstra, M., Hougee, M., 2020a. Riverbank macrolitter in the Dutch Rhine-Meuse delta. Environ. Res. Lett. 15 (10) https://doi.org/10.1088/1748-9326/ABB2C6.

van Emmerik, T., Vriend, P. and Roebroek, J. 2020b. An evaluation of the River-OSPAR method for quantifying macrolitter on Dutch riverbanks. Available at: https://research.wur.nl/en/publications/an-evaluation-of-the-river-ospar-method-for-quantifying-macrolitt.

van Rijn, L.C., 1984. Sediment transport, part i: bed load transport. J. Hydraul. Eng. 110 (10), 1431–1456. Available at. http://ascelibrary.org/doi/10.1061/%28ASCE%290733-9429%281984%29110%3A10%281431%29.

Dick Vethaak, A., Legler, J., 2021. Microplastics and human health. Science 371 (6530), 672–674 (1979)Available at. https://www.science.org/doi/10.1126/science.abe5041.

Voth, G.A., Soldati, A., 2017. Anisotropic particles in turbulence. Annu Rev. Fluid. Mech. 49 (1), 249–276. Available at. https://www.annualreviews.org/doi/10.1146/annurev-fluid-010816-060135.

Vriend, P., van Calcar, C., Kooi, M., Landman, H., Pikaar, R., van Emmerik, T., 2020. Rapid assessment of floating macroplastic transport in the Rhine. Front. Mar. Sci. 7 https://doi.org/10.3389/fmars.2020.00010.

Vriend, P., Schoor, M., Rus, M., Oswald, S.B., Collas, F.P.L., 2023. Macroplastic concentrations in the water column of the river Rhine increase with higher discharge. Sci. Total Environ. 900, 165716. Available at: https://linkinghub.elsevier.com/retrieve/pii/S0048969723043395.

Wadell, H., 1932. Volume, shape, and roundness of rock particles. J. Geol. 40 (5), 443–451. https://doi.org/10.1086/623964.

Waldschläger, K., Schüttrumpf, H., 2019. Effects of particle properties on the settling and rise velocities of microplastics in freshwater under laboratory conditions. Environ. Sci. Technol. 53 (4), 1958–1966. Available at: https://pubs.acs.org/doi/full/10.1021/acs.est.8b06794.

Waldschläger, K., et al., 2022. Learning from natural sediments to tackle microplastics challenges: a multidisciplinary perspective. Earth Sci. Rev. 228, 104021. Available at: https://linkinghub.elsevier.com/retrieve/pii/S0012825222001052.

Wilks, D.S., 2006. Statistical methods in the atmospheric sciences. Elsevier Sci. Available at https://books.google.co.uk/books?id=_vSwyt8_OGEC.

Yu, Z., Loewen, M., Guo, S., Guo, Z., Zhang, W., 2023. Investigation of the sheltering effects on the mobilization of microplastics in open-channel flow. Environ. Sci. Technol. 57 (30), 11259–11266. https://doi.org/10.1021/acs.est.3c02500.